https://dx.doi.org/10.1016/j.ymssp.2022.109766

Acoustical performance of a wavy micro-perforated panel absorber

Weiping Yang, Yatsze Choy*, Ying Li

Department of Mechanical Engineering, The Hong Kong Polytechnic University, Hung Hom, Kowloon, Hong Kong SAR, People's Republic of China

* Corresponding author.
E-mail address: mmyschoy@polyu.edu.hk (Y. S. Choy).

Abstract

In this study, the sound absorption performance of a wavy micro-perforated panel absorber (WMPPA) is investigated. First, a numerical model is established to calculate the sound absorption coefficients of micro-perforated panel absorbers (MPPAs) under normal, oblique, and random incidences. Subsequently, the proposed model is validated using an existing theoretical formula. After that, the acoustical properties of a WMPPA are explored and then compared with those of flat and corrugated micro-perforated panel absorbers (FMPPAs, CMPPAs). It is observed that the normal sound absorption curve of WMPPA shifts to a lower frequency range compared with those of CMPPA and FMPPA, which is promising for the control of low-frequency noise. Besides, the sound absorption performance of the WMPPA at the dips is considerably improved, which is favourable for the reduction of broadband noise. Modal analysis shows that, apart from the resonant mode, the adjacent non-resonating modes are also excited, which enhances the performance. Moreover, the WMPPA exhibits the properties of a multiple-layered MPPA, and extra sound absorption peaks are observed within the middle- to high-frequency range. In addition, a parametric study is conducted to explore the influence of the corrugation depth and offset distance on the sound absorption performance of the WMPPA. The calculated results demonstrate that the proposed WMPPA is suitable for low-frequency and broadband noise control. Furthermore, a compact WMPPA with a high random sound absorption coefficient is obtained following an optimization scheme. Finally, the sound absorption coefficients of the MPPAs under normal plane-wave incidence are obtained experimentally using an impedance tube. The measurement results agree well with the simulation results, validating the proposed model and verifying some of the numerical findings.

Keywords: Sound absorption coefficient; Oblique incidence; Micro-perforated panel absorber; Wavy structure

1. Introduction

Micro-perforated panel absorbers (MPPAs) have been extensively adopted to attenuate architectural and environmental noise [1-3]. A conventional MPPA is assembled by installing a micro-perforated panel (MPP) in front of a rectangular and empty backing cavity [4]. As MPPs can be manufactured from a variety of materials, such as metals, plastics, and wood, they can be used in duct systems, indoor or outdoor environments. For example, Kang and Brocklesby [2] proposed the use of transparent MPPs in window systems to maintain ventilation efficiency and attenuate environmental noise. Asdrubali and Pispola [3] designed an innovative sound barrier using a transparent polycarbonate MPP, which exhibited excellent performance in both acoustical and optical fields. Besides, Wu [5] designed duct silencers by placing parallel-arranged MPPs inside a duct, which showed good performance owing to optimum duct geometry and MPP parameters. Subsequently, new types of mufflers [6] and dissipative silencers [7] have been developed for duct noise applications. To control room noise, Dupont et al. [8] proposed lightweight MPPs backed by flexible panels to reduce sound transmission between rooms. MPPAs can also be adopted to attenuate noise in magnetic resonance imaging scanners, protect the hearing of patients, and reduce their discomfort [9]. These examples demonstrate that MPPAs can be applied in different environments.

Owing to the potential of MPPAs in the noise-control field, many efforts have been made to improve the acoustical performance of MPPAs. Liu and Herrin [10, 11] attempted to improve the sound absorption of MPPAs using partitioned or honeycomb-structured backing cavities, and the overall insertion loss was increased. To widen the working frequency bandwidth, an MPPA with a trapezoidal backing cavity that alters the coupling effects between the MPP and irregularly-shaped cavity was developed [12]. To improve low-frequency sound absorption and achieve extra resonances, an L-shaped backing cavity [13] and Helmholtz resonator integrated with MPP [14, 15] were developed. In addition to modifying the design of the backing cavities in MPPAs, flexible structures were introduced to improve the performance of

MPPAs. Lee et al. [16] investigated the vibration effects of flexible panels on the sound absorption performance of MPPAs. Bravo et al. [17, 18] theoretically and experimentally determined the sound absorption properties of MPPAs and improved them by incorporating a flexible panel. To achieve a wide frequency bandwidth of noise reduction in the low-frequency regime, researchers have developed a plate silencer composed of light MPPs with moderate bending stiffness to mass ratio [19, 20]. The plate silencer reflects and absorbs the sound waves inside the duct by vibroacoustic coupling among the sound fields in the duct and MPP structures. Another plate silencer was also designed by integrating tubing structures which further widened the working frequency bandwidth [21, 22]. In addition, various design concepts of MPPAs, such as multiple-layered MPPs inside a backing cavity [23-28], an array of MPPAs in parallel arrangement [29-32], and an MPPA array in a serial-parallel coupling manner [33] have been proposed to improve sound absorption performance. In general, MPPAs with different sub-cavity depths in a parallel arrangement can provide wider sound absorption bandwidths than those in serial arrangements. To further widen the sound absorption bandwidth of MPPAs, inhomogeneous MPPs have been proposed [34-36]. A favourable sound absorption bandwidth can be achieved by optimizing the parameters of sub-MPPs in inhomogeneous MPPAs.

The aforementioned MPPAs have been widely applied in engineering, and they exhibit excellent sound absorption ability under normal plane-wave incidence. However, their in-situ performance in complex acoustical environments is unsatisfactory [37, 38]. Therefore, for practical applications, the sound absorption performance of MPPAs subjected to oblique and random incidences has been studied [39-40]. The sound absorption properties of a conventional MPPA with a flat MPP and rectangular cavity are defined by the mass-spring system consisting of air inside the micro-perforations and backing cavity. However, its sound absorption properties vary with the incident angle because of the change in the equivalent acoustical impedance of the MPPA with different incident angles [41]. Besides, in an MPPA

with a rectangular cavity, only the acoustical modes normal to the MPP contribute to the sound absorption performance. Hence, the performance of FMPPA may be restricted at some frequencies. To mitigate these shortcomings, a corrugated MPPA (CMPPA) has been proposed. The CMPPA changes the incident angle of the incoming sound waves on the local MPP surface and creates an irregularly-shaped backing cavity which enables more acoustical modes to contribute to the sound absorption performance of the CMPPA [42]. Previous studies have demonstrated that multiple acoustical modes of the CMPPA are excited at the peak and dip frequencies. Besides, the acoustical responses of the non-resonating modes improve the sound absorption performance of the CMPPA. Therefore, it can be concluded that CMPPAs possess favourable properties for broadband random noise control and can be effectively applied to noise attenuation devices in complex acoustical environments such as buildings, traffic tunnels, and factory plants. However, the potential of CMPPA is limited by the fixed sinusoidal MPP profile. Therefore, in this study, a WMPPA is proposed for mitigating the limitations caused by the fixed sinusoidal MPP profile in CMPPA. The absorption of higher-order acoustical modes, which can facilitate the broadband noise attenuation in complex acoustical environments, is analysed and enhanced. In addition to the advantages of the CMPPA, the proposed WMPPA is more versatile, exhibits good performance in the low-frequency range, and presents excellent broadband sound absorption ability within the middle- to high-frequency range.

The primary objectives of this study are as follows: (1) to establish a numerical model for calculating the sound absorption coefficients of MPPAs under normal, oblique, and random incidences; (2) to validate the proposed model using formulas and experiments; (3) to analyse the acoustical properties of the proposed WMPPA and investigate the mechanisms behind its sound absorption performance; (4) to develop a compact WMPPA with optimum broadband random sound absorption performance. The remainder of this paper is organized as follows. In Section 2, a numerical model is proposed to evaluate

the oblique sound absorption performance of MPPAs. In Section 3, the proposed model is validated, and the sound absorption performance of the WMPPA is investigated. In Section 4, experimental studies to verify the numerical model are presented. Finally, the conclusions are drawn in Section 5.

2. Numerical model

A schematic diagram of a WMPPA under oblique plane-wave incidence is shown in Fig. 1. As a wavy MPP could be arbitrarily designed, and the optimized WMPP profile remains unknown, we start with a Z-shaped WMPPA. The properties of a Z-shaped WMPP are characterized by a four-point interpolation curve, which can be determined by the width (W), corrugation depth (H), and offset distance (O). Thus, it can be inferred that the air gap between the WMPP and the bottom surface of the WMPPA forms an irregularly-shaped backing cavity, and the cavity depth varies. Therefore, the distance from the middle surface of the WMPP to the bottom is defined as the cavity depth (D). In this regard, the cavity volume of the WMPPA is the same as that of a flat micro-perforated panel absorber (FMPPA).

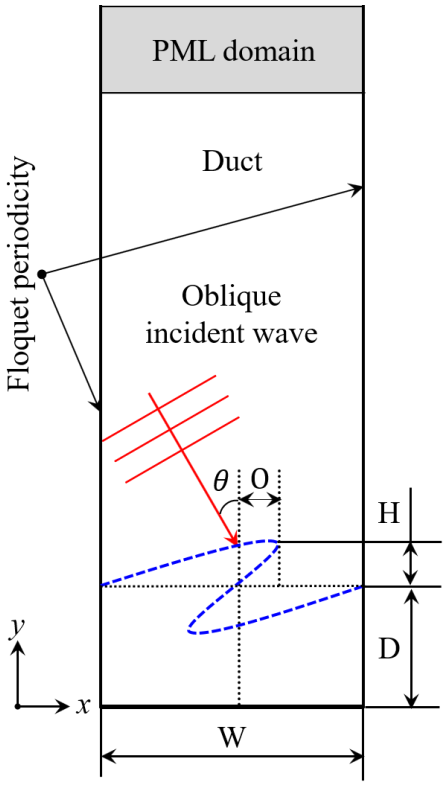

Fig. 1 Schematic diagram of a wavy micro-perforated panel absorber under oblique plane-wave incidence.

Suppose a plane acoustical wave with unit amplitude is incident obliquely on a WMPP. The incident sound pressure field is expressed as follows:

$$p_{incident} = e^{-ik(\sin\theta x - \cos\theta y)}, \tag{1}$$

where k denotes the wavenumber in the free space, $i = \sqrt{-1}$ is the imaginary unit, and θ is the incident angle. A part of the incident sound energy is reflected or scattered by the WMPP, and the rest is dissipated by the proposed WMPPA. For an FMPP, the acoustical impedance is determined by Maa's equation [4]:

$$Z_{MPP} = \frac{32\eta t_{MPP}}{p_{MPP} d_{MPP}^2}\left(\sqrt{1+\frac{K^2}{32}} + \frac{\sqrt{2}}{32} K \frac{d_{MPP}}{t_{MPP}}\right) + \frac{i\rho\omega t_{MPP}}{p_{MPP}}\left(1 + \frac{1}{\sqrt{9+K^2/2}} + 0.85\frac{d_{MPP}}{t_{MPP}}\right), \tag{2}$$

where $K = d_{MPP}\sqrt{\omega\rho/4\eta}$ with η being the coefficient of viscosity. The panel thickness, orifice diameter, and perforation ratio of the MPP are denoted by t_{MPP}, d_{MPP}, and p_{MPP}, respectively. Note that Eq. (2) is used to obtain the average acoustical impedance of each orifice over the MPP surface. Because a WMPP can be formed by reshaping an FMPP, the local acoustical impedance over the wavy profile is the same as that of an FMPP. However, the actual length and perforation area of a WMPP are longer and larger than those of an FMPP of the same width. Hence, to keep the perforation area the same for all MPPs, the perforation ratio of a WMPP is calculated using the following equation:

$$p_{WMPP} = \frac{W}{L_{WMPP}} p_{FMPP}, \tag{3}$$

where L_{WMPP} denotes the arc length of the WMPP.

In the frequency domain, the sound pressure fields in the virtue duct and backing cavity satisfy the Helmholtz equation:

$$\left(\nabla^2 + k^2\right) p = 0\,, \tag{4}$$

where $\nabla^2 = \partial^2/\partial x^2 + \partial^2/\partial y^2$ denotes the two-dimensional (2D) Laplace operator. For both sides of the WMPP, the acoustical particle velocity in the direction normal to the local surface is given by

$$u_n = \frac{p_{cavity} - p_{duct}}{Z_{MPP}}, \tag{5}$$

where n denotes the direction normal to the local surface. To account for the infinite size of the MPPA system, periodic boundary conditions are applied on two sides of the backing cavity and duct, which are described as follows:

$$p_L = p_R e^{-ik\sin\theta W}\,, \tag{6}$$

where the subscripts 'L' and 'R' denote the left and right boundaries, respectively. For the inlet of the virtue duct, a Dirichlet-to-Neumann (DtN) boundary condition can be applied to mimic the non-reflection boundary [42]. Alternatively, a perfectly matched layer (PML) can be adopted for the simulation. For the bottom wall, a rigid boundary condition is applied as follows:

$$\left.\frac{\partial p}{\partial y}\right|_{y=-D} = 0\,. \tag{7}$$

The Helmholtz equation and relevant boundary conditions are solved using the commercial software package COMSOL Multiphysics. The 'Background pressure field' is used to represent the oblique incidence plane-wave, as shown in Eq. (1). The boundary condition stated in Eq. (5) is implemented by specifying the 'Interior impedance' which is determined by Eq. (2) on the WMPP. The periodic boundary conditions are applied using the 'Floquet periodicity'. Finally, the bottom side of the backing cavity is defined as 'Acoustically rigid wall' as demonstrated in Eq. (7). In the finite element model, at least eight elements per wavelength are generated to ensure calculation accuracy. In addition, a PML is imposed on the top of the virtual duct to simulate a non-reflection boundary.

After obtaining the sound pressure field, the oblique sound absorption coefficient of the WMPPA is calculated as follows:

$$\alpha_\theta = \frac{-\rho c_0 \int_{inlet} \mathrm{Re}\left(p u_y^*\right) dx}{W \cos\theta}, \tag{8}$$

where the asterisk denotes the complex conjugate. The sound absorption coefficient under a random incidence is calculated by

$$\alpha_r = \int_0^{\pi/2} \alpha_\theta \sin\left(2\theta\right) d\theta \,. \tag{9}$$

The developed model is employed to investigate the sound absorption performance of the WMPPAs as shown in Fig. 2 (b) and Fig. 2 (d). Besides, the acoustical properties of an FMPPA and CMPPA are also evaluated for comparison, as demonstrated in Fig. 2 (a) and Fig. 2 (c), respectively. However, to maintain cavity volumes the same as the FMPPA, the profiles of the CMPPA and WMPPA are protruded outwards for a corrugation depth, which increases the thickness of the corrugated MPPAs. To obtain a more compact absorber, the acoustical performance of a WMPPA with the same height as the FMPPA is also investigated, as shown in Fig. 2 (b). This configuration results in a decrease of the cavity volume. However, the corrugation depth and offset distance are changeable, which may provide unexpected performance by optimizing the geometrical parameters of the WMPP.

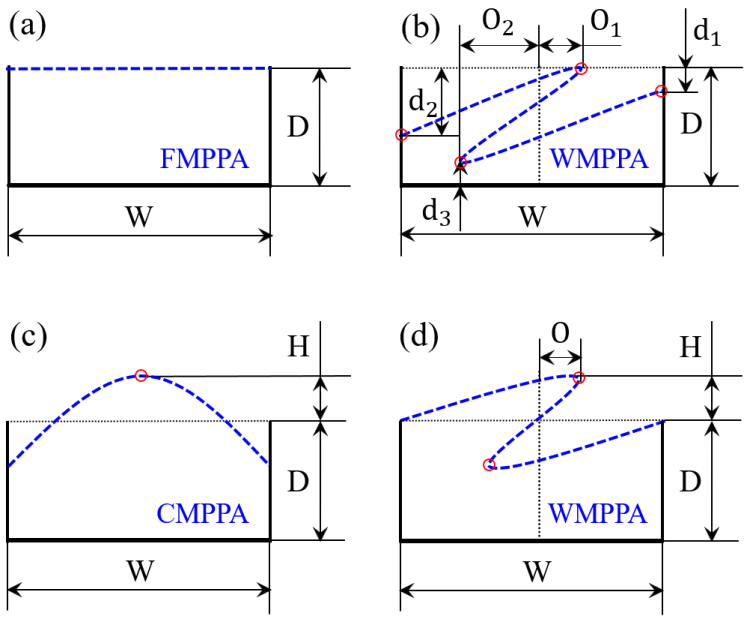

Fig. 2 Different configurations of MPPAs. (a) an FMPPA, (b) a WMPPA with the same height as the FMPPA, (c) an CMPPA with the same volume as the FMPPA, (d) a WMPPA with the same volume as the FMPPA.

3. Results and discussions

In this section, the proposed numerical model is validated using a theoretical formula, and the acoustical properties of the WMPPA are investigated. The cavity depth of the CMPPA, described in Ref. [42], was 200 mm which is unsuitable for practical applications. Therefore, in this study, the following default parameters are used:

$$\begin{aligned} &W=100\ \text{mm},\ D=100\ \text{mm},\ H=25\ \text{mm},\ O=25\ \text{mm},\\ &d_{MPP}=0.4\ \text{mm},\ t_{MPP}=0.4\ \text{mm},\ p_{FMPP}=1\%. \end{aligned} \tag{10}$$

Besides, the speed of sound and density of air are 340 m/s and 1.225 kg/m^3, respectively.

3.1. Model validation using theoretical formulas

The sound absorption coefficient of an FMPPA under oblique plane-wave incidence is estimated as follows:

$$\alpha_\theta = \frac{4\,\mathrm{Re}\left(Z_{FMPPA}\right)\cos\theta}{\left[1+\mathrm{Re}\left(Z_{FMPPA}\right)\cos\theta\right]^2+\left[\mathrm{Im}\left(Z_{FMPPA}\right)\cos\theta\right]^2} \tag{11}$$

where Z_{FMPPA} represents the acoustical impedance of the FMPPA (with or without sub-cavities), which can be obtained using the equivalent circuit method. To validate the proposed model applying Eq. (11), three cases are considered: (a) a normal plane-wave incidence on an FMPPA, (b) an oblique (45°) plane-wave incidence on an FMPPA, and (c) an oblique (45°) plane-wave incidence on an FMPPA with sub-cavities. The cavity depth of the single FMPPA is 100 mm, and the depths of the sub-cavities in the FMPPA with sub-cavities are 100 mm, 50 mm, 12 mm, and 25 mm. As presented in Fig. 3 (a) and Fig. 3 (b), under both normal and oblique plane-wave incidences, the results obtained using the numerical method agree well with those calculated using Eq. (11). However, in Fig. 3 (c), discrepancies can be observed between the results obtained using the proposed method and Eq. (11) under oblique plane-wave incidence. The oblique sound absorption coefficient of an FMPPA array is a function of the geometrical size of the sub-cavities and incidence angle. However, Eq. (11) only considers the effect of the incident angle, and the effects of the other parameters are ignored. Thus, only a specific configuration is described by Eq. (11), i.e., the sizes of the sub-cavities are infinitesimal compared with the acoustical wavelength. Therefore, only approximate values of the sound absorption coefficient of an MPPA with sub-cavities under oblique plane-wave incidence can be obtained using Eq. (11). Accurate numerical approaches such as the proposed approach are necessary for the evaluation of the actual acoustical performance of an MPPA array.

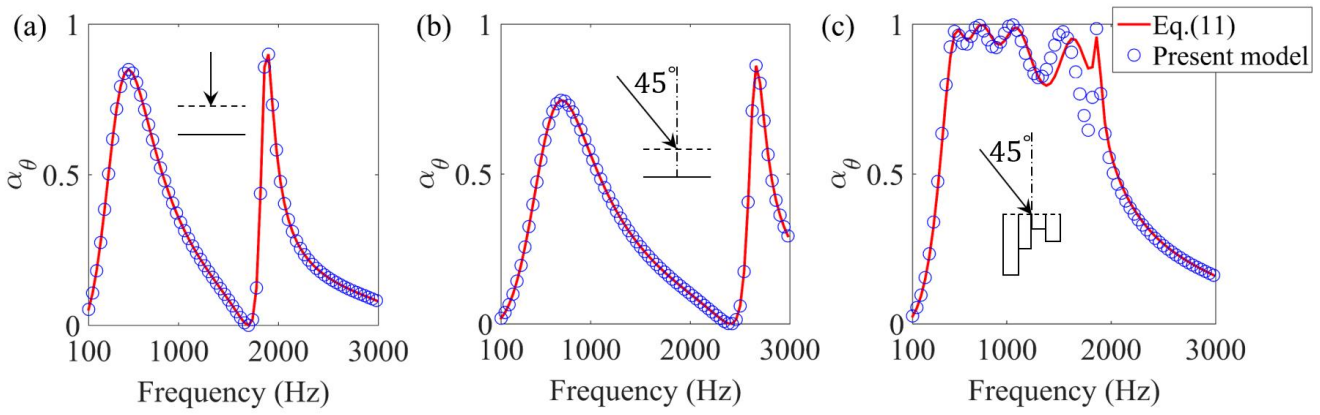

Fig. 3 Sound absorption coefficients of MPPAs: (a) normal plane-wave incidence on an FMPPA, (b) oblique (45°) plane-wave incidence on the FMPPA, and (c) oblique (45°) plane-wave incidence on an MPPA with sub-cavities.

3.2. Acoustical properties of WMPPAs

The sound absorption coefficients of FMPPA, CMPPA, and WMPPA under normal plane-wave incidence are compared in Fig. 4. The sound absorption coefficient of the WMPPA at the first trough (1075 Hz) is improved compared with that of the CMPPA (1580 Hz) and FMPPA (1700 Hz). This is advantageous for broadband attenuation of a highly reverberated acoustical field. The first sound absorption peak of the WMPPA shifts to a lower frequency (385 Hz) compared with that of the FMPPA and CMPPA (500 Hz) which is promising for the control of low-frequency noise. Besides, there are three sound absorption peaks between the frequency ranges of 1500 Hz and 2300 Hz which also improves the sound absorption performance of the WMPPA in the middle- to high- frequency range. In addition, considering the ratio of the corrugation depth to the wavelength of the incident sound wave, it can be inferred that the CMPPA performs almost the same as the FMPPA below approximately 700 Hz. However, the performance of the WMPPA is not influenced by the ratio in this frequency range.

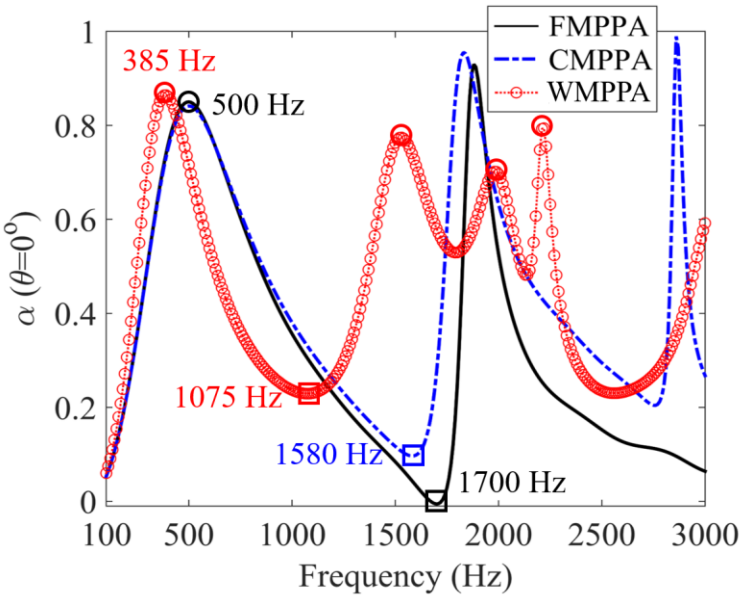

Fig. 4 Normal sound absorption coefficients of the FMPPA, CMPPA, and WMPPA.

The dips in the sound absorption coefficient curve of the MPPA can be attributed to the resonances of the backing cavity. At the resonant frequencies of a cavity, the stiffness of the air gap becomes infinity. Consequently, the air inside the perforations cannot vibrate, and no energy dissipation occurs. The shapes of the first three non-zero modes and the corresponding eigenfrequencies of the FMPPA, CMPPA, and WMPPA are demonstrated in Fig. 5. For the FMPPA, the first resonant frequency of the cavity is located at 1700 Hz, and the sound pressure along the FMPP is large. Thus, no sound energy is absorbed, which results in the dip of the sound absorption coefficient. For the CMPPA, the first resonant frequency is 1573 Hz. The sound pressure along the CMPP is large, however, it exhibits a decreasing trend towards the two sides. Therefore, a part of the sound energy is absorbed in these regions, and the first dip in the sound absorption coefficient curve increases. For the WMPPA, the first resonant frequency of the cavity is 1165 Hz. However, the cavity is partitioned into two parts by the WMPP. The sound pressure in the upper part of the sub-cavity is large, however, the sound pressure along the lower part of the WMPP is moderate, which allows more sound energy absorption. Therefore, the sound absorption coefficient of WMPPA at

the first dip is enhanced considerably compared with those of FMPPA and CMPPA. In addition, the first dip of the FMPPA is located at 1700 Hz, which is the same as the resonant frequency of the cavity. This implies that only the resonant mode contributes to the sound absorption performance of the FMPPA at 1700 Hz. However, for the CMPPA and WMPPA, the frequencies of the first troughs shift compared with the resonant frequencies of the cavities. Thus, it can be concluded that that apart from the dominant mode, some adjacent acoustical modes also contribute to the sound absorption performance.

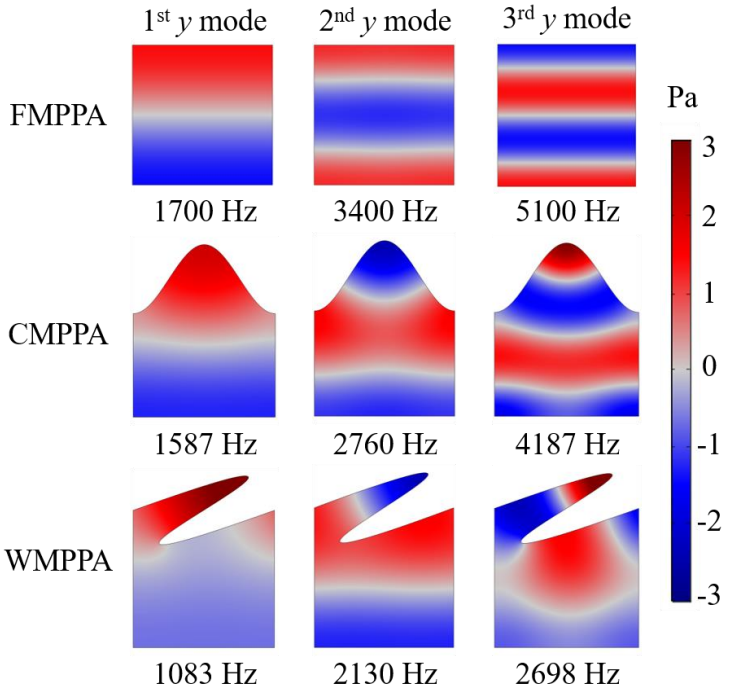

Fig. 5 The shapes of the first three nonzero cavity modes along *y* direction and the corresponding eigenfrequencies of the FMPPA, CMPPA, and WMPPA with the same volume.

These properties are also reflected by the sound pressure and sound intensity fields inside the MPPAs, as demonstrated in Fig. 6. For the FMPPA, at 1700 Hz, the distribution pattern of the sound pressure inside the cavity is the same as the first modal shape. In the first modal shape of the FMPPA, the sound pressure along the MPP surface is huge, and the sound energy is completely reflected. As a result, no sound

absorption occurs. For the CMPPA, at 1580 Hz, the sound pressure on the top of the CMPP is large, which blocks part of the incident sound energy. However, the sound pressure on the two sides is moderate, which enables the CMPPA to absorb sound waves. For the WMPPA, at 1075 Hz, the sound pressure at the sharp corner is large. Most of the incident sound waves enter the cavity via the rest of the WMPP surface and be dissipated. Therefore, the introduction of the WMPP profile changes the modal properties of the irregularly-shaped cavity and alters the sound pressure distribution inside the WMPPA which is formed not only by the resonant mode but also adjacent modes. These non-resonant modes contribute to the improvement of the sound absorption performance at the dip frequency. Furthermore, the WMPP profile also plays the role of a multi-layered MPP, which introduces multiple peaks in the middle- to high-frequency range. Although the second sound absorption peak of the FMPPA and CMPPA is larger than that of the WMPPA. The bandwidth of the peaks for half sound absorption is narrow. The second to fourth sound absorption peaks of the WMPPA are not as high as those of the FMPPA and CMPPA, however, the frequency band of half sound absorption is wide, which is favourable for broadband sound reduction.

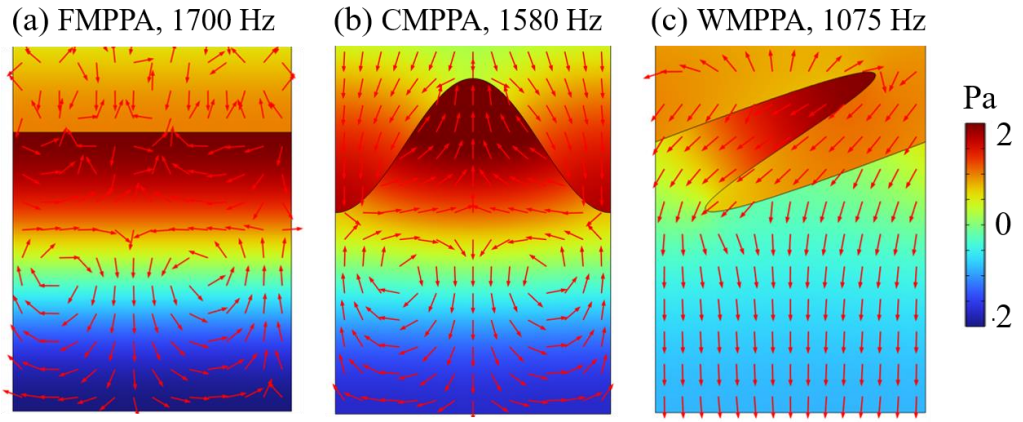

Fig. 6 Sound pressure (contour) and sound intensity (arrows) inside MPPAs at their dip frequencies: (a) FMPPA at 1700 Hz, (b) CMPPA at 1580 Hz, and (c) WMPPA at 1075 Hz.

To further explore the modal contributions behind the sound absorption performance of the MPPAs, modal analysis is implemented. The sound pressure field inside the irregularly-shaped baking cavity is expanded in terms of acoustical modes as follows:

$$p = \sum_{m=0}^{\infty} A_m \phi_m, m = 0,1,2,\ldots, \tag{12}$$

where ϕ_m denotes the mode shape, and A_m is the modal response coefficient which can be calculated after determining the sound pressure field inside the cavity as follows:

$$A_m = \frac{\iint_S p\phi_m^* dS}{\iint_S \phi_m \phi_m^* dS}, m = 0,1,2,\ldots, \tag{13}$$

where S refers to the cavity volume and the asterisk denotes complex conjugate.

The normalized modal response coefficients of the backing cavities in FMPPA, CMPPA, and WMPPA at their first peak and dip frequencies are shown in Fig. 7. For the CMPPA and WMPPA, there always be a dominant acoustical mode at each peak and dip frequency, together with multiple adjacent acoustical modes that also contribute significantly to the sound field. Moreover, with increasing non-resonating modal contributions, the dip of the sound absorption curve improves. Thus, the multi-mode response of the irregularly-shaped configuration is different from that of the flat configuration, in which only the resonating mode contributes to the sound pressure field at the dip frequency. As a result, there is no sound absorption at 1700 Hz for the FMPPA.

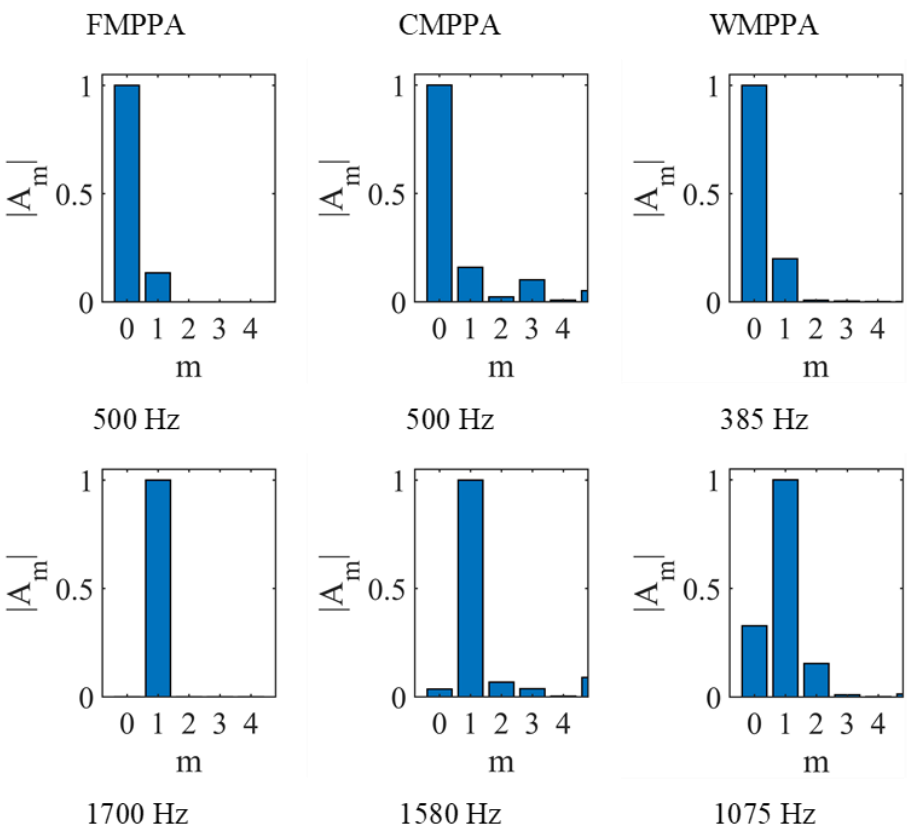

Fig. 7 Modal response coefficients of the backing cavities of FMPPA, CMPPA, and WMPPA at their first peak and trough frequencies.

The sound absorption coefficients of the FMPPA, CMPPA, and WMPPA under oblique plane-wave incidences are demonstrated in Fig. 8. As shown in Fig. 8 (a), at an incident angle of 30°, apart from the low-frequency shift of the first peak and sound absorption enhancement of the first trough, the peaks in the sound absorption coefficient curve of the WMPPA between 1500 Hz and 2000 Hz improve considerably compared with the case of normal-incidence. The first trough almost disappears at an incident angle of 60° even though the first peak decreases, as demonstrated in Fig. 8 (b). The sound absorption coefficients are larger than 0.5 in the frequency range of 500 Hz to 1850 Hz, and the performance of the WMPPA is superior to that of the FMPPA and CMPPA under 800 Hz. As displayed

in Fig. 8 (c), at an incident angle of 85°, approximately no sound absorption by the FMPPA is observed. However, the CMPPA and WMPPA could still absorb sound energy owing to the curved MPP profiles, and the WMPPA exhibits better performance than the CMPPA.

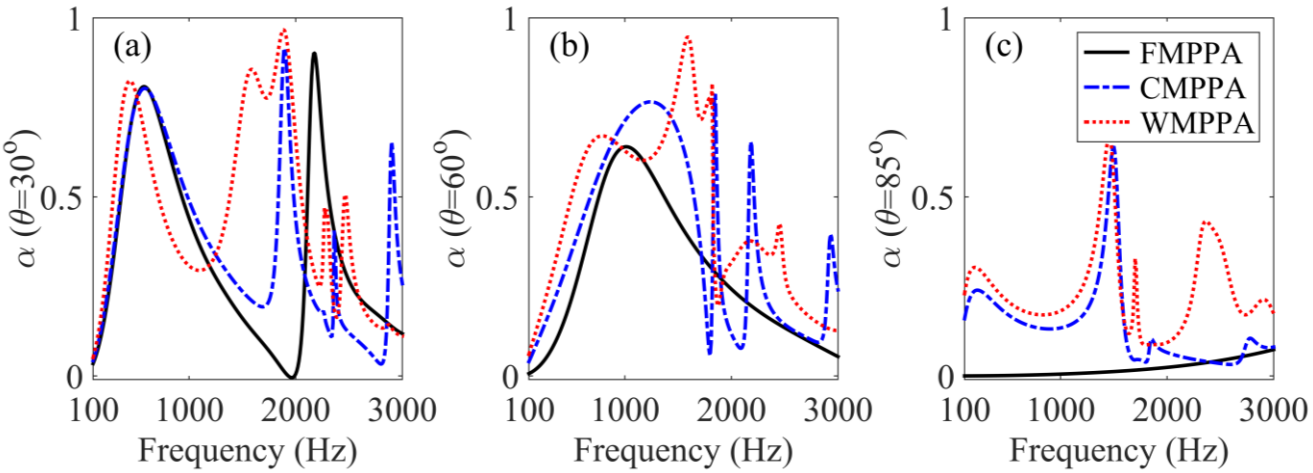

Fig. 8 Oblique sound absorption coefficients of the FMPPA, CMPPA, and WMPPA at an incident angle of (a) 30°, (b) 60°, and (c) 85°.

It is observed that with increasing incident angle, the sound absorption curves shift to higher frequencies. MPPs react locally, and their acoustical impedances are independent of the incident angle. However, the acoustical impedances of the cavities vary with the incident angle, which causes a shift in the sound absorption coefficient curve. From the above analysis, it can be concluded that the sound absorption performance of the curved MPPAs under oblique plane-wave incidence is better than that of their normal counterparts, especially at large incident angles. In addition, it is observed that the sound absorption coefficients of the WMPPA and CMPPA improve significantly under oblique plane-wave incidence. However, the FMPPA exhibits poor sound absorption performance under oblique plane-wave incidence, especially at large incident angles. The superior sound absorption performance of the WMPPA and CMPPA is due to the local incident angle of the plane sound wave, which does not change in the same

pattern as the angle of the background sound field, as presented in Fig. 9. Note that when the incident angle of the background sound field reaches 90°, the sound wave propagates to the FMPP at a grazing angle, however, it propagates to the CMPP and WMPP at certain local incident angles.

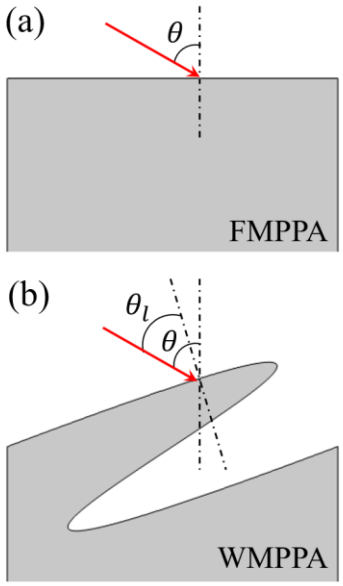

Fig. 9 Oblique incident angle and the local incident angle on the MPP surfaces: (a) FMPPA and (b) WMPPA.

3.3 Parametric studies

As discussed in Section 3.2, the WMPP profile, which is characterized by the offset distance, acts as a multi-layered MPPA. Therefore, the effect of the offset distance (O) on the oblique sound absorption coefficient of the WMPPA is investigated. The changes in the oblique sound absorption coefficient with respect to the offset distance are shown in Fig. 10. At an incident angle of 0°, the first sound absorption peak shifts to a lower frequency with increasing offset distance, along with a decrease in the bandwidth. This is also observed for an incident angle of 30°. Besides, double peaks are observed when the offset distance exceeds 20 mm. At an incident angle of 60°, the first sound absorption peak decreases, however,

the bandwidth increases remarkably. In addition, double sound absorption peaks can be observed in the frequency range of 1200 Hz to 1800 Hz. The frequency interval between these peaks decreases with increasing offset distance. At an incident angle of 85°, sound absorption only occurs in a small frequency band, and the peak increase with increasing offset distance.

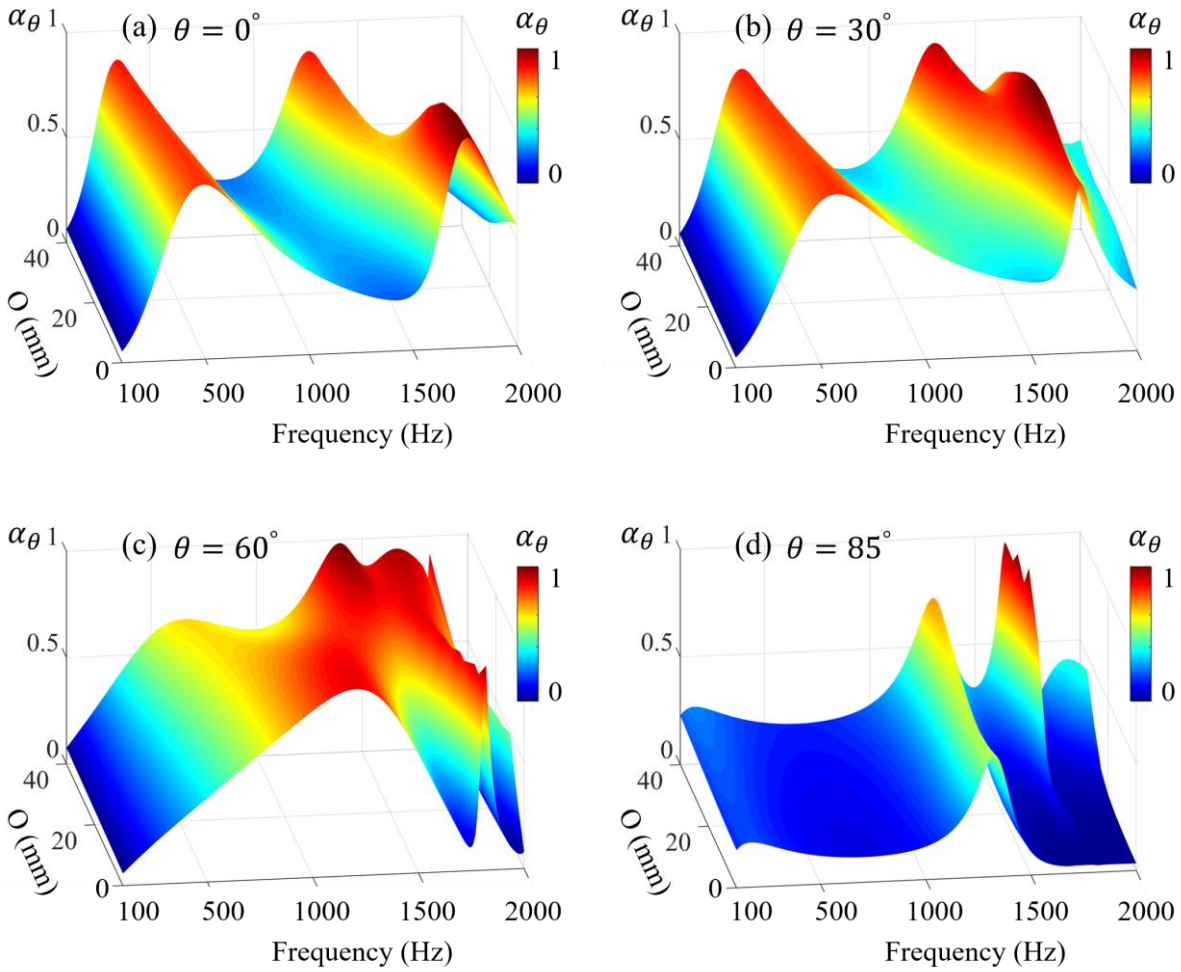

Fig. 10 Influence of the offset distance on the oblique sound absorption coefficient of WMPPA at an incident angle of (a) 0°, (b) 30°, (c) 60°, and (d) 85°, respectively.

Another significant parameter that influences the sound absorption performance of a WMPPA is the corrugation depth. Keeping the other parameters constant, the changes in the sound absorption coefficients

with respect to the corrugation depth are demonstrated in Fig. 11. At incident angles of 0° and 30°, the first sound absorption peaks decrease slightly and shift to higher frequencies with increasing corrugation depth, Furthermore, the first sound absorption dips and the second sound absorption peaks improve with increasing corrugation depth. At an incident angle of 60°, the dips almost disappear which are replaced by a broadband sound absorption curve. Besides, the WMPPA achieves perfect sound absorption at the first peak when the corrugation depth is larger than 60 mm. At an incident angle of 85°, the corrugation depth has a negligible effect on the sound absorption coefficient of the WMPPA.

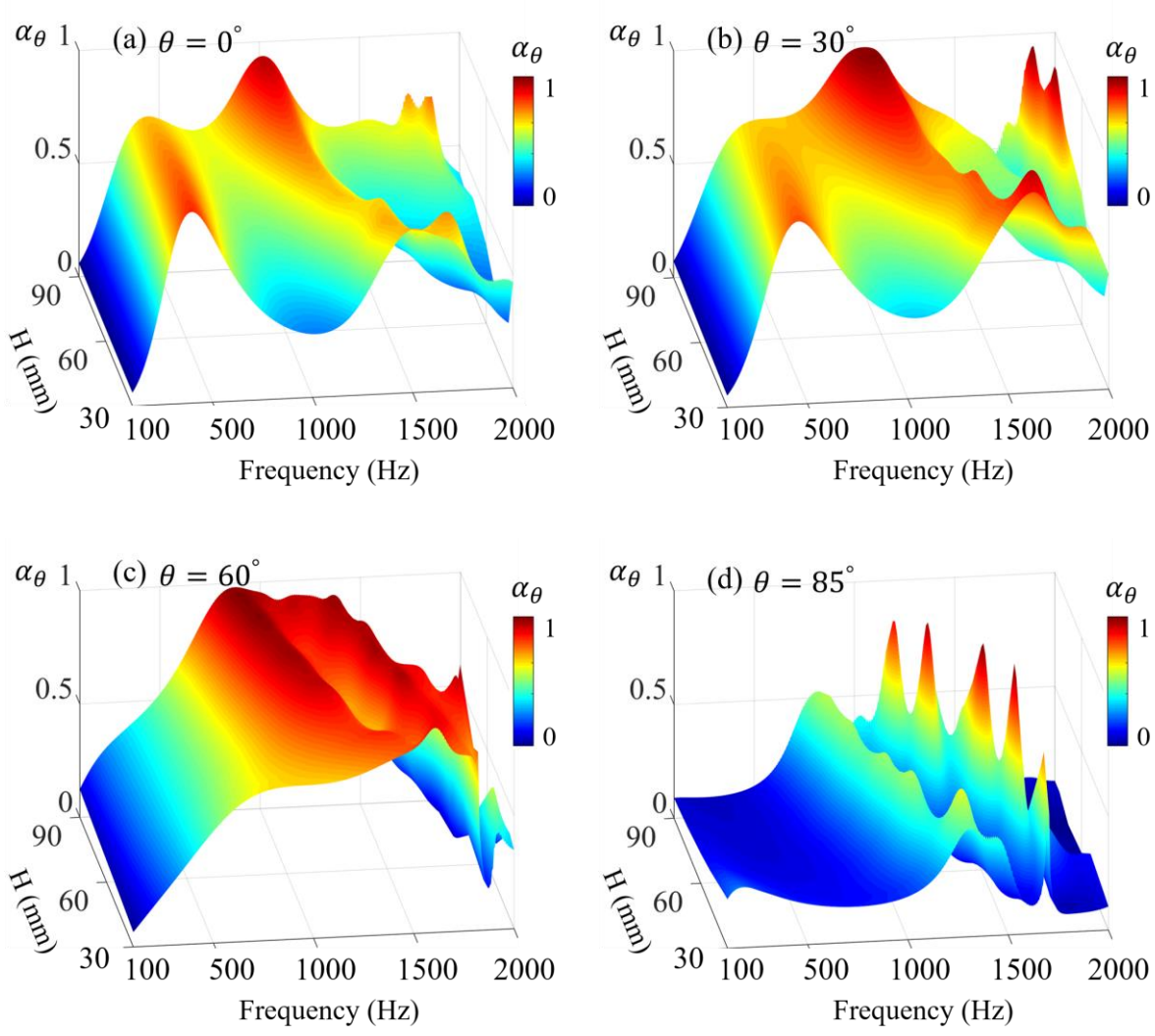

Fig. 11 The effect of corrugation depth on the oblique sound absorption coefficient of WMPPA at an incident angle of (a) 0°, (b) 30°, (c) 60°, and (d) 85°, respectively.

3.4 Random sound absorption coefficients

In a complex acoustical environment, incident sound waves propagate to MPPAs at random angles. Therefore, the random sound absorption coefficients of the FMPPA, CMPPA, and WMPPA are obtained and compared in Fig. 12. Within the frequency range considered, the WMPPA and CMPPA perform better than the FMPPA. This can be attributed to the fact that the corrugated MPPAs perform better than the FMPPA at both normal and oblique plane-wave incidences, as presented in the preceding sections. The random sound absorption coefficients of the WMPPA are almost larger than those of the CMPPA, particularly in the frequency range of 1000 Hz to 1800 Hz. This can be attributed to the flexibility of the WMPP, which forms several sub-cavities that can achieve multiple peaks in the sound absorption curve in middle- to high-frequency range. In general, the WMPPA provides a broadband half random sound absorption curve in the frequency range of 400 Hz to 1400 Hz, which is the most common frequency range of environmental noise.

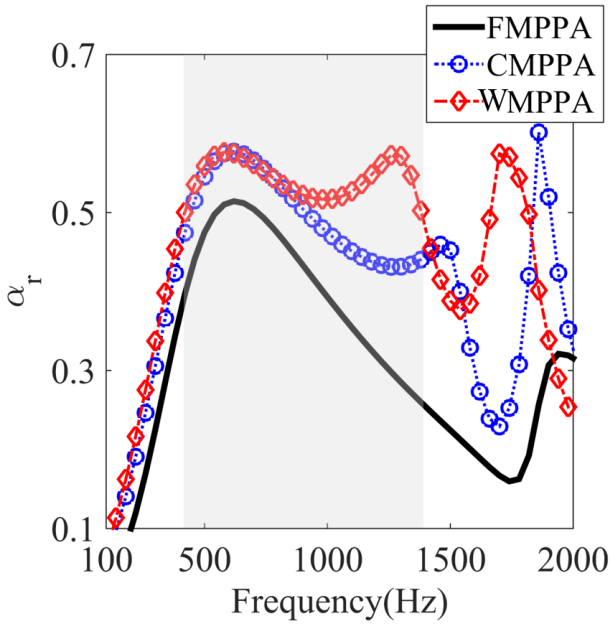

Fig. 12 Comparisons of the random sound absorption coefficients between the FMPPA, CMPPA, and WMPPA.

3.5 Optimized compact WMPPA

The cavity volumes of the MPPAs are maintained the same to make fair comparisons in the above analyses. However, CMPPA and WMPPA occupy more space than FMPPA owing to the protruding corrugation profiles, which is not favourable for compact noise control devices. Therefore, the acoustical properties of a WMPPA and a CMPPA with heights the same as that of an FMPPA are investigated.

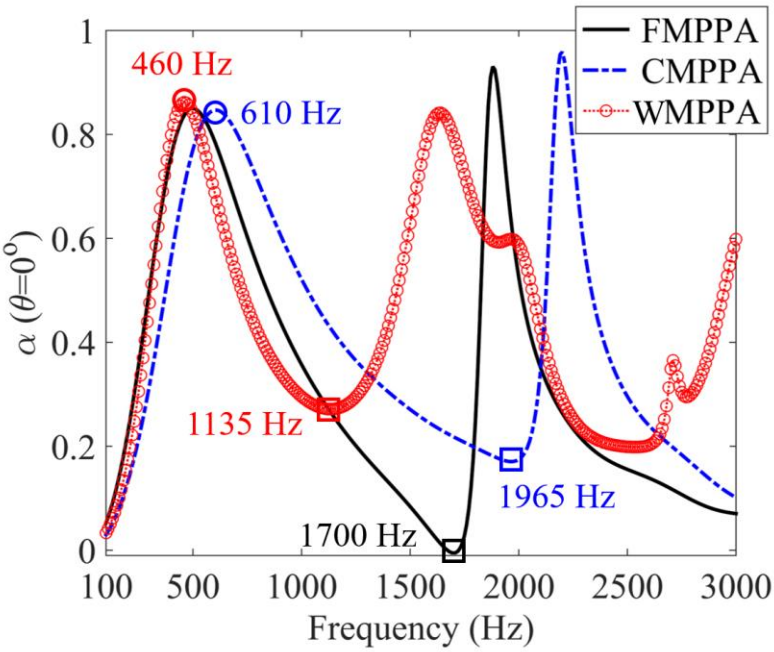

Fig. 13 Sound absorption coefficients of the FMPPA, CMPPA, and WMPPA with the same height under a normal plane-wave incidence.

The sound absorption coefficients of the FMPPA, CMPPA, and WMPPA under a normal plane-wave incidence are shown in Fig. 13. As the heights of the MPPAs are kept the same, the cavity volumes of the CMPPA and WMPPA are smaller than that of the FMPPA. Consequently, for CMPPA, the first dip of the sound absorption coefficient curve shifts to a higher frequency (1965 Hz) compared with 1580 Hz in Fig. 4. Similarly, for the WMPPA, the first dip shifts to a higher frequency (1135 Hz) compared with

1075 Hz in Fig. 4. However, the first dip of the WMPPA is still at a lower frequency than that of the FMPPA (1700 Hz), which results from the offset distance of the WMPP profile. This phenomenon is also observed at the first peaks of the CMPPA and WMPPA, and the frequencies shift to 610 Hz and 460 Hz, respectively. However, for the WMPPA, the first peak frequency is still lower than that of the FMPPA (500 Hz). Therefore, it can be concluded that the offset distance of the WMPPA compensates for the frequency shift caused by the lower volume. In addition, the broadband sound absorption performance in the middle- to high-frequency range remains unaffected.

The sound absorption coefficients of the FMPPA, CMPPA, and WMPPA under oblique plane-wave incidence (30°) are presented in Fig. 14. These results are similar to those shown in Fig. 8. The primary difference between them is that the sound absorption curves of the compact CMPPA and WMPPA shift to higher frequencies owing to the lowering of the volume. However, the WMPPA exhibits superior performance compared with the CMPPA, which can be attributed to the WMPP profile, especially the offset distance.

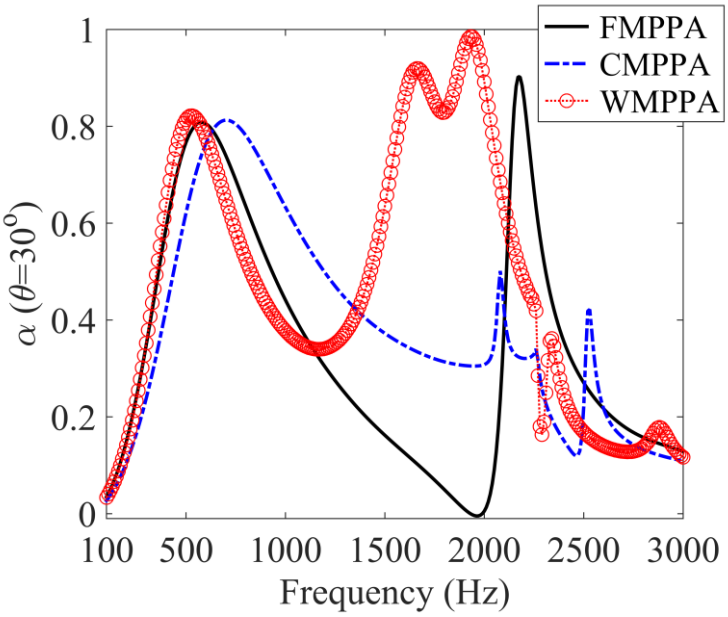

Fig. 14 Oblique sound absorption coefficients of FMPPA, CMPPA, and WMPPA of the same height at an incident angle of 30°.

The effect of the offset distance on the oblique sound absorption coefficient of the WMPPA with the same height as the FMPPA is demonstrated in Fig. 15. In the case of normal incidence, with increasing offset distance, the characteristic of low-frequency shift exhibits. The amplitudes of the sound absorption peaks increase as well. In the case of oblique incidence (45°), two peaks are observed in the middle-frequency range.

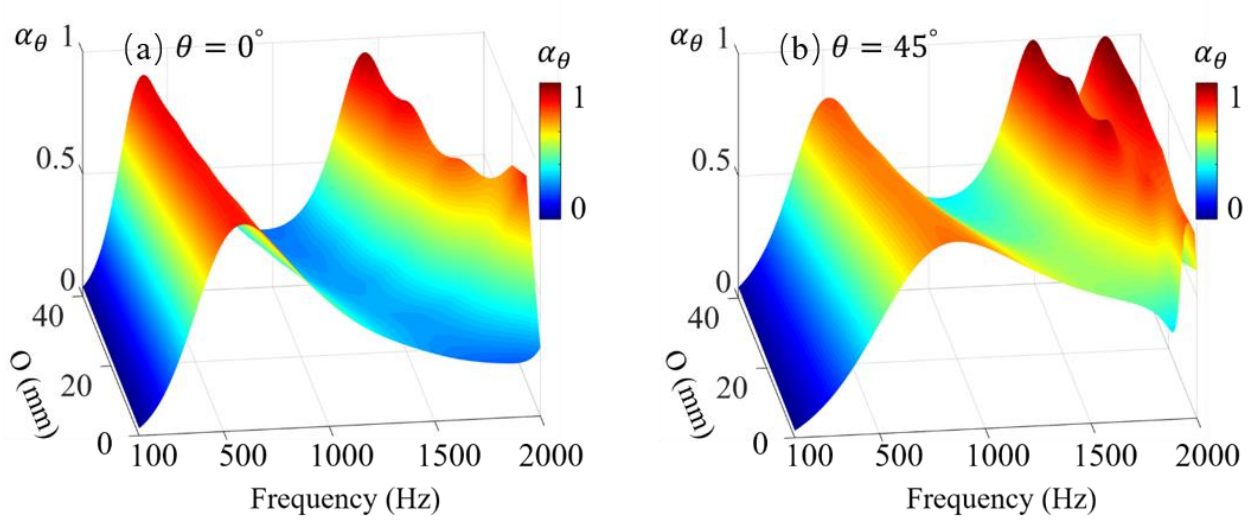

Fig. 15 Effect of the offset distance on the sound absorption coefficient of a WMPPA with the same height as the FMPPA, (a) at normal incidence, (b) at oblique incidence (45°).

The presented results are obtained using the default parameters. Based on the parametric study, the performance of the WMPPA can be optimized. However, various configurations can be used to meet the requirements of different practical applications. Combining COMSOL and MATLAB, we first tune the MPP parameters to guarantee that the sound absorption coefficient reaches 1 at the first peak. By filtering the results, we choose the panel thickness, hole diameter, and perforation ratio to be 2 mm, 4 mm, and 1.2%, respectively. Then, using these MPP parameters, we optimize the offset distance to be 30 mm so that the half random sound absorption bandwidth is the broadest in the middle-frequency range of 300 Hz

to 2000 Hz. Under these optimized configurations, the normal and oblique (30°, 45°) sound absorption coefficients of the WMPPA are presented in Fig. 16.

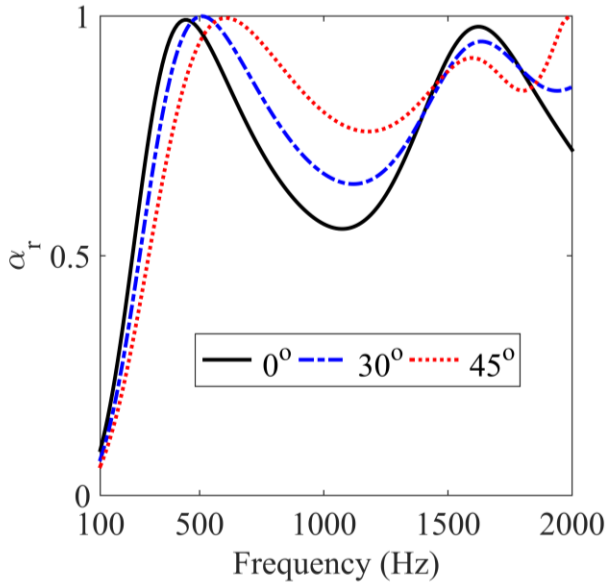

Fig. 16 The normal and oblique (30°, 45°) sound absorption coefficients of WMPPA under the optimized configurations.

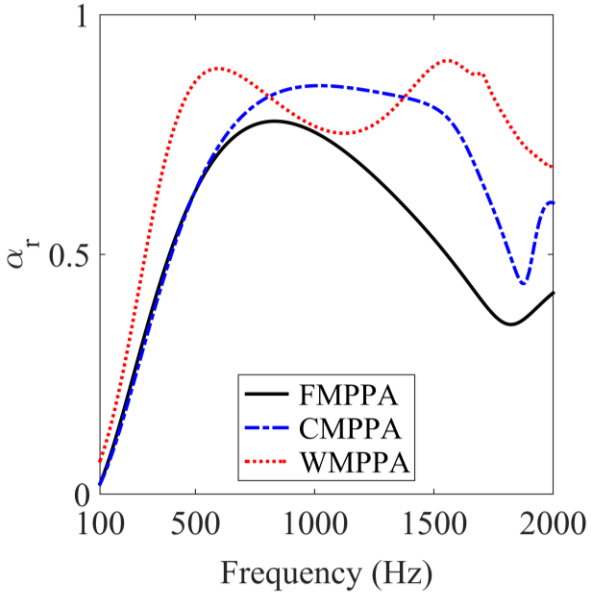

Fig. 17 Comparison of the random sound absorption coefficients between FMPPA, CMPPA, and WMPPA.

The random sound absorption coefficients of the WMPPA are calculated and compared with those of CMPPA and FMPPA, as shown in Fig. 17. From these figures, a compact WMPPA is obtained, which not only can provide full sound absorption at the first peak under oblique plane-wave incidence but also possesses a broadband half sound absorption performance within the frequency range of 300 Hz to 2000 Hz. The compact WMPPA performs better than the FMPPA and CMPPA at random incidence. Thus, the proposed compact WMPPA can be used for broadband sound absorption. Note that the optimized performance of WMPPA is obtained using the Z-shaped WMPP profile. A more promising configuration of WMPPA can be explored applying the topology optimization [43-45].

4. Experimental validation

The sound absorption coefficients of the FMPPA, CMPPA, and WMPPA under normal plane-wave incidence are measured by applying the two-microphone transfer-function method. A schematic diagram of the experimental setup is demonstrated in Fig. 18 (a). A sinusoidal signal is generated using the LabVIEW program. The generated signal is then converted by a digital-to-analogue convertor (DAC, NI PCI-M10-16E-1), amplified by a power amplifier (B&K Lab Gruppen 300), and played by a loudspeaker. The cross-section of the duct is 100×100 mm^2 which can maintain the plane-wave condition under 1700 Hz. The acoustical signals inside the rectangular duct are recorded by a pair of microphones (B&K type 4947). Subsequently, the acoustical signals are amplified by a conditioning amplifier (B&K Nexus 2693) and digitized by an analogue-to-digital convertor (ADC, NI PCI-4452). The testing system is controlled by a LabVIEW program, which has the advantages of excellent stability and real-time performance.

The FMPPs are fabricated from stainless steel using the etching technique. The profiles of the CMPP and WMPP are then obtained by reshaping the FMPP on prepared moulds, which are made using 3D printing, as demonstrated in Fig. 18 (b). The assembled MPPAs are mounted at the end of the duct using screws, and the gaps are sealed with glue, as shown in Fig. 18 (c). The thickness and hole diameter of the

FMPP are 0.2 mm and 0.3 mm, respectively. The corrugation depth of the CMPP and WMPP is 50 mm and the offset distance of the WMPP is 25 mm. Besides, the perforation ratio of the FMPP, CMPP, and WMPP are 0.4%, 0.17%, and 0.13%, respectively. The normal sound absorption coefficients obtained from the numerical model and experiments are compared in Fig. 19. From the figure, it can be observed that the numerical and experimental results are in good agreement. For the FMPPA and CMPPA, as shown in Fig. 19 (a) and Fig. 19 (b), the experiment presents higher sound absorption coefficients than the numerical predictions, especially when the frequency is above about 700 Hz which is caused by the system error of the test rig according to our previous experience. However, in Fig. 19 (c), a big discrepancy is observed between the experimental and numerical results for the WMPPA. This is caused by the shape error of the WMPP as it is hard to reshape the FMPP to WMPP permanently by the prepared moulds. The WMPP deformed during the sealing and mounting procedures which results in errors.

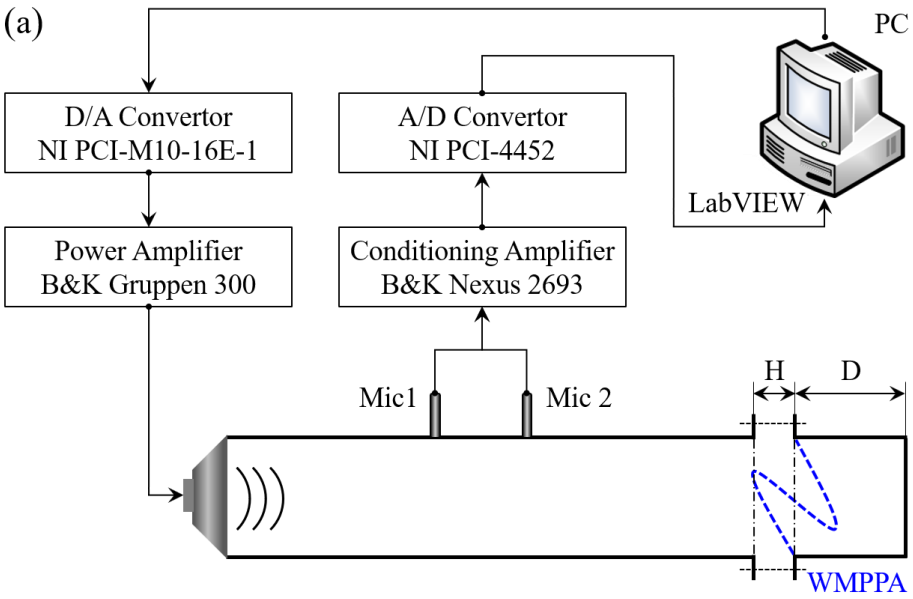

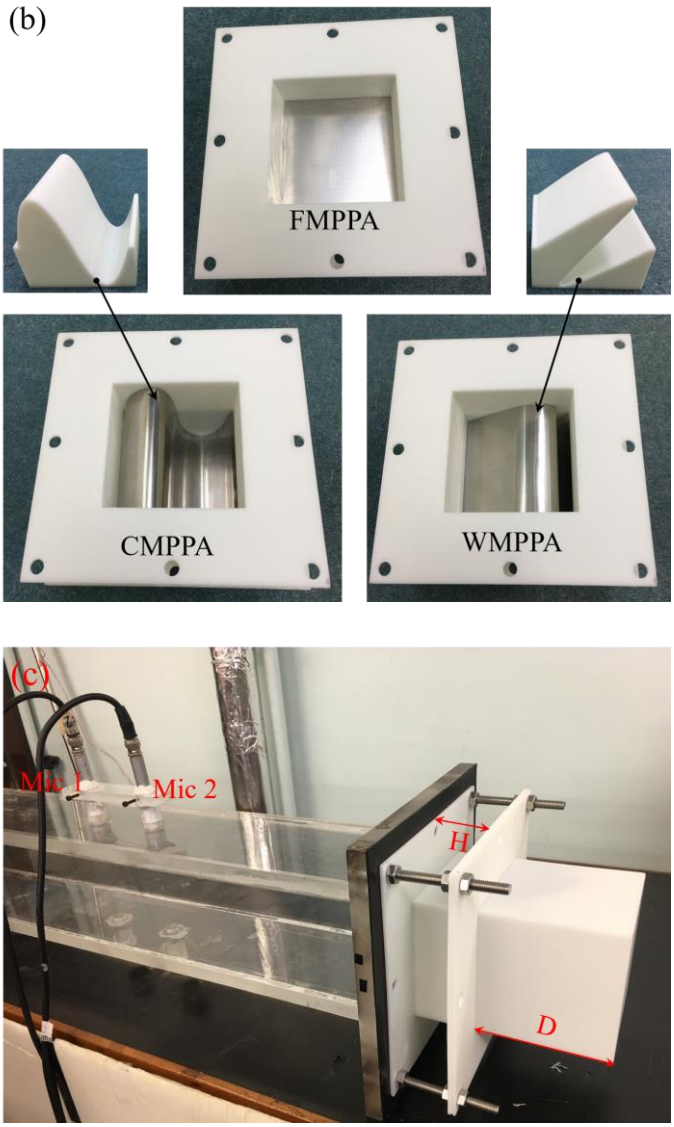

Fig. 18 Experimental setup for the measurement of the normal sound absorption coefficients of MPPAs: (a) schematic diagram, (b) photography of MPPAs and moulds, and (c) photography of the test rig.

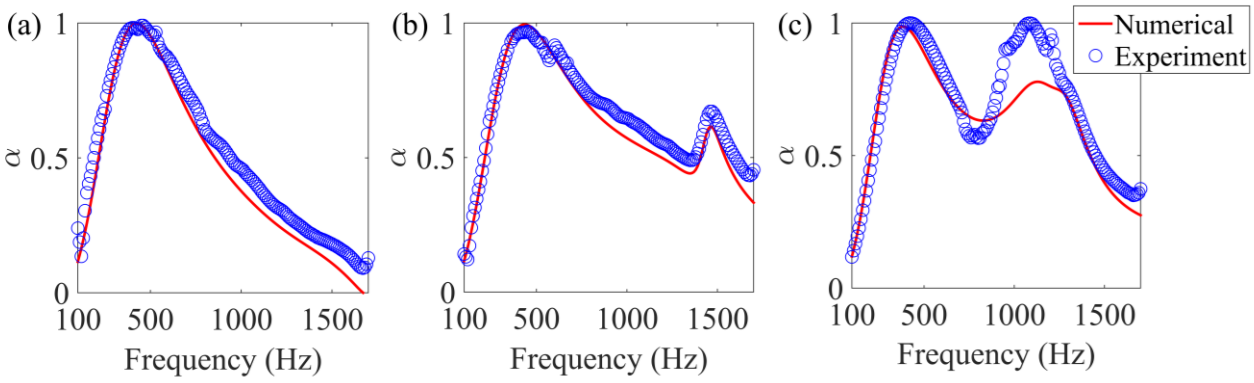

Fig. 19 Normal sound absorption coefficients obtained by the numerical model and experiments. (a) FMPPA, (b) CMPPA, and (c) WMPPA.

5. Conclusions

In this study, the sound absorption performance of a WMPPA under normal, oblique, and random incidences is investigated numerically and experimentally. The WMPP exhibits the advantages of the suppression of noise within a wide frequency range, elimination of the dip frequency, and efficient sound reduction at oblique incidence angles. Based on the results obtained, the following conclusions can be drawn:

(1) The sound absorption properties of a WMPPA are different from those of a traditional FMPPA owing to the irregular WMPP profile. It is observed that the normal sound absorption coefficients of WMPPA at dip frequencies improved significantly compared with those of the CMPPA and FMPPA. This can be attributed to the contribution of the multiple non-resonating modes, as demonstrated by the modal analysis. In addition, The WMPPA exhibits sound absorption peaks in the middle- to high-frequency range. This is due to the introduction of the offset distance, which forms an irregular backing cavity that performs like a multiple-layered MPPA.

(2) The sound absorption performance of the WMPPA and CMPPA is superior to that of the FMPPA under oblique plane-wave incidence, especially at large incident angles. For corrugated MPPs, the local incident angle does not follow the same change pattern as the global incident angle. At large incident angles, the FMPPA almost loses its sound absorption ability. However, the WMPPA exhibits good sound performance.

(3) Under random incidences, the WMPPA and CMPPA perform better than the FMPPA within the frequency range considered in this study. The random sound absorption coefficients of the WMPPA are almost larger than those of the CMPPA, especially in the frequency range of 1000 Hz to 1800 Hz. These characteristics can ensure a broad half sound absorption and are favourable for broadband random noise control.

(4) The sound absorption coefficients of the FMPPA, CMPPA, and WMPPA are measured under normal plane-wave incidence using an impedance tube. The measured results agree well with the numerical predictions which validates the proposed model.

Acknowledgements

The authors would like to acknowledge the funding support from the Research Grants Council, Hong Kong (PolyU15209520).

References

[1] H. V. Fuchs, X. Zha, Micro-perforated structures as sound absorbers-a review and outlook, Acta Acust. United Ac. 92 (1) (2006) 139-146.

[2] J. Kang, M. W. Brocklesby, Feasibility of applying micro-perforated absorbers in acoustic window systems, Appl. Acoust. 66 (6) (2005) 669-689.

[3] F. Asdrubali, G. Pispola, Properties of transparent sound-absorbing panels for use in noise barriers, J. Acoust. Soc. Am. 121 (1) (2007) 214-221.

[4] D. Y. Maa, Potential of microperforated panel absorber, J. Acoust. Soc. Am. 104 (5) (1998) 2861-2866.

[5] M. Q. Wu, Micro-perforated panels for duct silencing, Noise Control Eng. J. 45 (2) (1997) 69-77.

[6] S. Allam, M. Abom, A new type of muffler based on microperforated tubes, J. Vib. Acoust. 133 (3) (2011) 031005.

[7] M. Abom, S. Allam, Dissipative silencers based on micro-perforated plates, SAE Tech. Pap. 2013-24-0071 (2013).

[8] T. Dupont, G. Pavic, B. Laulagnet, Acoustic properties of lightweight micro-perforated plate systems, Acta Acust. United Ac. 89 (2) (2003) 201-212.

[9] G. Li, C. K. Mechefske, A comprehensive experimental study of micro-perforated panel acoustic absorbers in MRI scanners, Magn. Reson. Mater. Phys, Biol. Med. 23 (3) (2010) 177-185.

[10] J. Liu, D. W. Herrin, Enhancing micro-perforated panel attenuation by partitioning the adjoining cavity, Appl. Acoust. 71 (2) (2010) 120-127.

[11] D. Herrin, J. Liu, A. Seybert, Properties and applications of microperforated panels. Sound Vib. 45 (7) (2011) 6-9.

[12] C. Wang, L. Cheng, J. Pan, G. Yu, Sound absorption of a micro-perforated panel backed by an irregular-shaped cavity, J. Acoust. Soc. Am. 127 (1) (2010) 238-246.

[13] X. L. Gai, T. Xing, X. H. Li, B. Zhang, F. Wang, Z. N. Cai, Y. Han, Sound absorption of microperforated panel with L shape division cavity structure, Appl. Acoust. 122 (2017) 41-50.

[14] S. H. Park, Acoustic properties of micro-perforated panel absorbers backed by Helmholtz resonators for the improvement of low-frequency sound absorption, J. Sound Vib. 332 (20) (2013) 4895-4911.

[15] K. Mahesh, R. S. Mini, Theoretical investigation on the acoustic performance of Helmholtz resonator integrated microperforated panel absorber, Appl. Acoust. 178 (2021) 108012.

[16] Y. Y. Lee, E. W. M. Lee, C. F. Ng, Sound absorption of a finite flexible micro-perforated panel backed by an air cavity, J. Sound Vib. 287 (1-2) (2005) 227-243.

[17] T. Bravo, C. Maury, C. Pinhede, Sound absorption and transmission through flexible micro-perforated panels backed by an air layer and a thin plate, J. Acoust. Soc. Am. 131 (5) (2012) 3853-3863.

[18] T. Bravo, C. Maury, C. Pinhede, Vibroacoustic properties of thin micro-perforated panel absorbers, J. Acoust. Soc. Am. 132 (2) (2012) 789-798.

[19] Y. S. Choy, Y. Liu, H. Y. Cheung, Q. Xi, K. T. Lau, Development of composite plate for compact silencer design, J. Sound Vib. 331 (10) (2012) 2348-2364.

[20] X. N. Wang, Y. S. Choy, L. Cheng, Hybrid noise control in a duct using a light micro-perforated plate, J. Acoust. Soc. Am. 132 (6) (2012) 3778-3787.

[21] Q. Xi, Y. S. Choy, L. Cheng, S. K. Tang, Noise control of dipole source by using micro-perforated panel housing, J. Sound Vib. 362 (2016) 39-55.

[22] Z. B. Wang, Y. K. Chiang, Y. S. Choy, C. Q. Wang, Q. Xi, Noise control for a dipole sound source using micro-perforated panel housing integrated with a Herschel-Quincke tube, Appl. Acoust. 148 (2019) 202-211.

[23] D. Y. Maa, Microperforated-panel wideband absorbers, Noise Control Eng. J. 29 (3) (1987) 77-84.

[24] D. H. Lee, Y. P. Kwon, Estimation of the absorption performance of multiple layer perforated panel systems by transfer matrix method, J. Sound Vib. 278 (4-5) (2004) 847-860.

[25] R. Shimokura, Y. Soeta, Characteristics of train noise in above-ground and underground stations with side and island platforms, J. Sound Vib. 330 (8) (2011) 1621-1633.

[26] T. Bravo, C. Maury, C. Pinhede, Absorption and transmission of boundary layer noise through flexible multi-layer micro-perforated structures, J. Sound Vib. 395 (2017) 201-223.

[27] D. Chang, F. Lu, W. Jin, B. Liu, Low-frequency sound absorptive properties of double-layer perforated plate under grazing flow, Appl. Acoust. 130 (2018) 115-123.

[28] F. Bucciarelli, G. M. Fierro, M. Meo, A multilayer microperforated panel prototype for broadband sound absorption at low frequencies, Appl. Acoust. 146 (2019) 134-144.

[29] C. Wang, L. Huang, On the acoustic properties of parallel arrangement of multiple micro-perforated panel absorbers with different cavity depths, J. Acoust. Soc. Am. 130 (1) (2011) 208-218.

[30] M. Yairi, K. Sakagami, K. Takebayashi, M. Morimoto, Excess sound absorption at normal incidence by two microperforated panel absorbers with different impedance, Acoust. Sci. Technol. 32 (5) (2011) 194-200.

[31] D. Li, D. Chang, B. Liu, Enhancing the low frequency sound absorption of a perforated panel by parallel-arranged extended tubes, Appl. Acoust. 102 (2016) 126-132.

[32] Y. K. Chiang, Y. S. Choy, Acoustic behaviors of the microperforated panel absorber array in nonlinear regime under moderate acoustic pressure excitation, J. Acoust. Soc. Am. 143 (1) (2018) 538-549.

[33] Y. J. Qian, J. Zhang, N. Sun, D. Y. Kong, X. X. Zhang, Pilot study on wideband sound absorber obtained by adopting a serial-parallel coupling manner. Appl. Acoust. 124 (2017) 48-51.

[34] I. Prasetiyo, J. Sarwono, I. Sihar, Study on inhomogeneous perforation thick micro-perforated panel sound absorbers, J. Mech. Eng. Sci. 10 (3) (2016) 2350-2362.

[35] A. I. Mosa, A. Putra, R. Ramlan, I. Prasetiyo, A. A. Esraa, Theoretical model of absorption coefficient of an inhomogeneous MPP absorber with multi-cavity depths, Appl. Acoust. 146 (2019) 409-419.

[36] A. I. Mosa, A. Putra, R. Ramlan, A. A. Esraa, Wideband sound absorption of a double-layer microperforated panel with inhomogeneous perforation, Appl. Acoust. 161 (2020) 107167.

[37] L. Maxit, C. Yang, L. Cheng, J. L. Guyader, Modeling of micro-perforated panels in a complex vibro-acoustic environment using patch transfer function approach, J. Acoust. Soc. Am. 131 (3) (2012) 2118-2130.

[38] C. Yang, L. Cheng, Sound absorption of microperforated panels inside compact acoustic enclosures, J. Sound Vib. 360 (2016) 140-155.

[39] C. Yang, L. Cheng, J. Pan, Absorption of oblique incidence sound by a finite micro-perforated panel absorber, J. Acoust. Soc. Am. 133 (1) (2013) 201-209.

[40] Y. Liu, Y. Zhang, K. Chen, X. Ma, Oblique incidence sound absorption of a hybrid structure using a micro-perforated panel and a planar actuator, Appl. Phys. Express 13 (5) (2020) 057001.

[41] C. Wang, L. Huang, Y. Zhang, Oblique incidence sound absorption of parallel arrangement of multiple micro-perforated panel absorbers in a periodic pattern, J. Sound Vib. 333 (25) (2014) 6828-6842.

[42] C. Wang, X. Liu, Investigation of the acoustic properties of corrugated micro-perforated panel backed by a rigid wall, Mech. Syst. Signal Pr. 140 (2020) 106699.

[43] Y. Noguchi, T. Yamada, K. Izui, S. Nishiwaki, Topology optimization for hyperbolic acoustic metamaterials using a high-frequency homogenization method, Comput. Methods Appl. Mech. Eng. 335 (2018) 419-471.

[44] Y. Chen, F. Meng, X. Huang, Creating acoustic topological insulators through topology optimization, Mech. Syst. Signal Pr. 146 (2021) 107054.

[45] J. Guo, X. Zhang, Y. Fang, Topology optimization design and experimental validation of an acoustic metasurface for reflected wavefront modulation, J. Sound Vib. 520 (2022) 116631.